Supplementary Figures

Cell Sorting

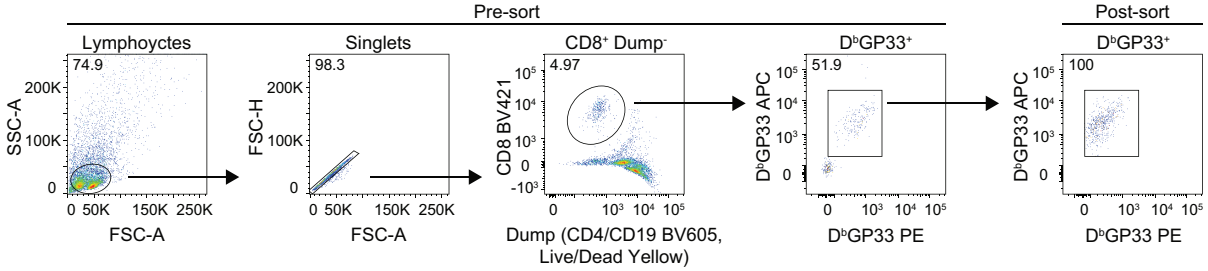

Supplementary Fig. 1. Gating strategy for sorting D^{b}GP33$^+$ CD8$^+$ T cells in Fig. 2, Fig. 4, Fig. 6d, e, Extended Data Fig. 3, and Extended Data Fig. 6. Splenocytes isolated from LCMV chronically infected of various treatment groups were gated on lymphocytes, singlets, live CD8$^+$ T cells, and D^{b}GP33$^+$ CD8$^+$ T cells were sorted.

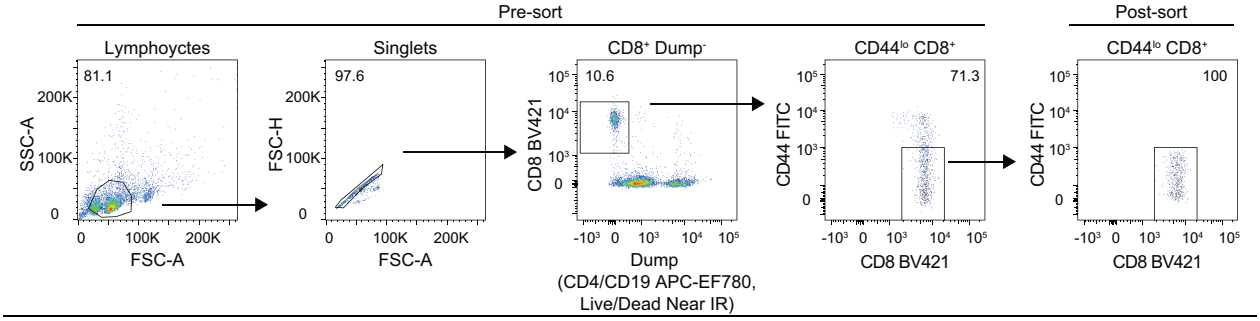

Supplementary Fig. 2. Gating strategy for sorting naive CD8$^+$ T cells in Fig. 2, 6d, and Extended Data Fig. 3. Splenocytes isolated from uninfected C57BL6/J mice were gated on lymphocytes, singlets, live CD8$^+$ T cells, and CD44^{lo} CD8$^+$ T cells were sorted. EF, eFluor.

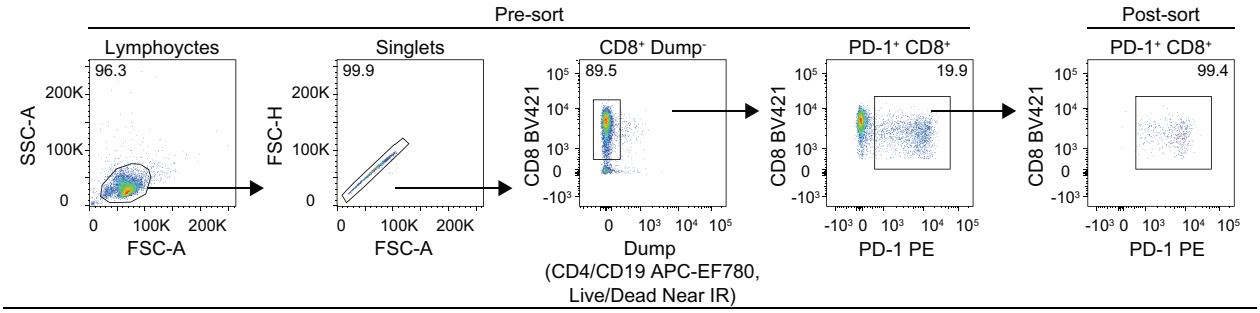

Supplementary Fig. 3. Gating strategy for sorting PD-1$^+$ CD8$^+$ T cells in Fig. 3f. Splenocytes isolated from LCMV chronically infected mice of various treatment groups were gated on lymphocytes, singlets, live CD8$^+$ T cells, and PD-1$^+$ CD8$^+$ T cells were sorted. EF, eFluor.

T cell analysis (CD8$^+$ T cells)

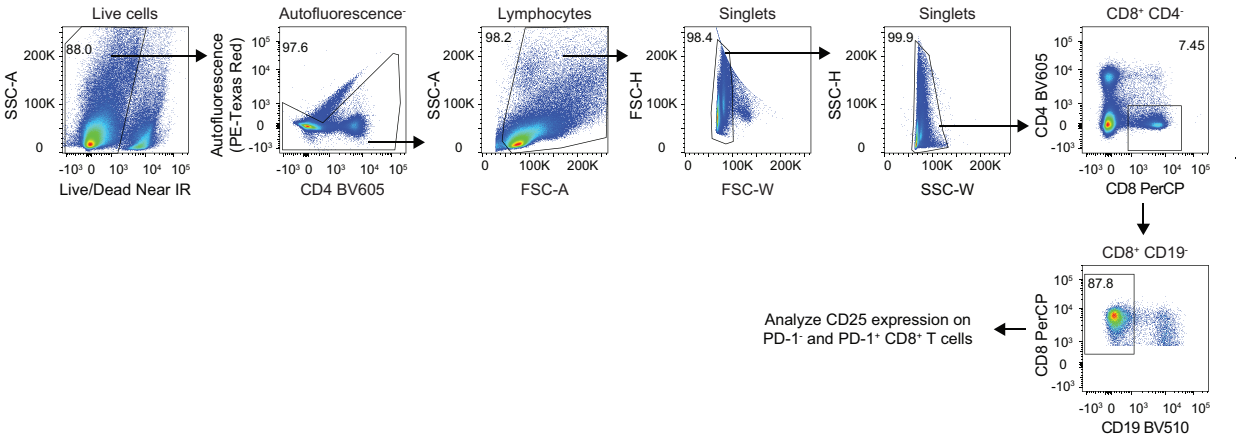

Supplementary Fig. 4. Gating strategy for CD8$^+$ T cells in Extended Data Fig. 12b, c. Splenocytes isolated from LCMV chronically infected mice of various treatment groups were gated on live cells, lymphocytes, singlets, autofluorescence$^-$ cells, CD8$^+$ T cells, and CD25 expression on PD-1$^-$ and PD-1$^+$ CD8$^+$ T cells were analyzed.

T cell analysis (LCMV-specific CD8$^+$ T cells, PD-1$^+$ CD8$^+$ T cells, naive CD44^{lo} CD8$^+$ T cells, LCMV-specific CD4$^+$ T cells, and Foxp3$^+$ CD4$^+$ T cells)

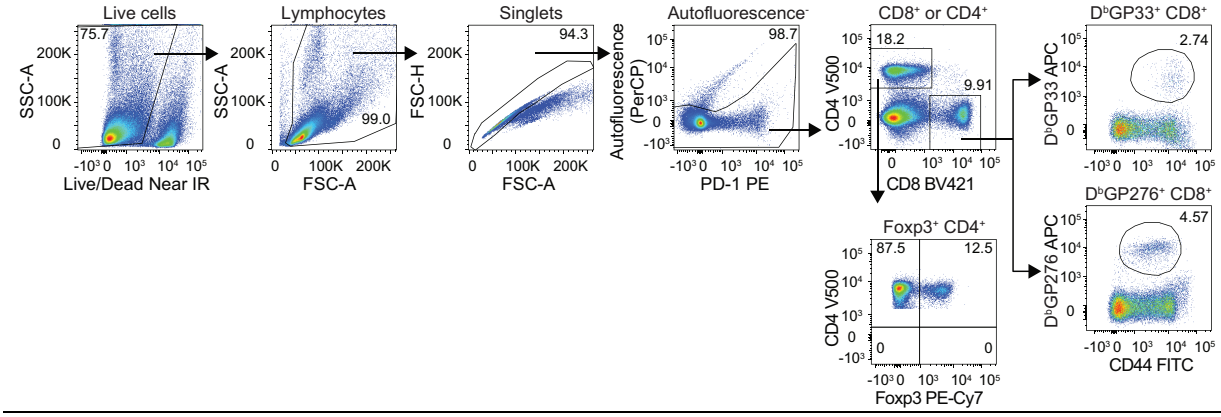

Supplementary Fig. 5. Gating strategy for LCMV-specific CD8$^+$ T cells and Foxp3$^+$ CD4$^+$ T cells in Fig. 5b, 6b, Extended Data Fig. 1b, 1h, 1i, 7b, 8, 10a, 10b, 11, and 13b. Cells isolated from various tissues in LCMV chronically infected mice of various treatment groups were gated on live cells, lymphocytes, singlets, autofluorescence$^-$ cells, CD8$^+$/CD4$^+$ T cells, and LCMV-specific D^{b}GP33$^+$ or D^{b}GP276$^+$ CD8$^+$ T cells or Foxp3$^+$ CD4$^+$ T cells were analyzed. For Fig. 1h, i, anti-CD8b.2 antibody was used to detect CD8$^+$ T cells.

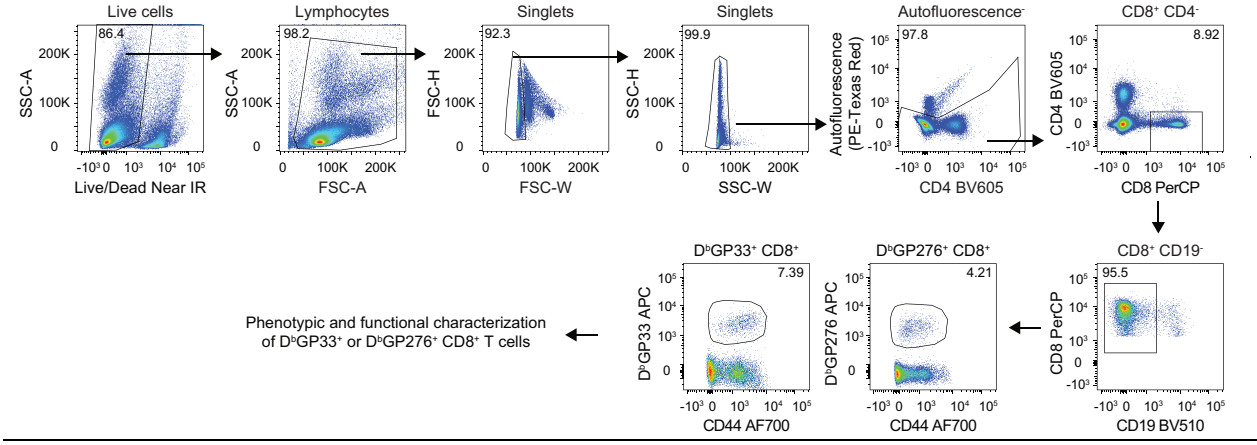

Supplementary Fig. 6. Gating strategy for LCMV-specific CD8$^+$ T cells in Fig. 5d, Extended Data Fig. 4, 9f, 9h, 9i, 9k, 9l, 9n, 9o, 10b, and 10d. Splenocytes isolated from LCMV chronically infected mice of various treatment groups were gated on live cells, lymphocytes, singlets, autofluorescence$^-$ cells, CD8$^+$ T cells, and LCMV-specific D^{b}GP33$^+$ or D^{b}GP276$^+$ CD8$^+$ T cells were analyzed. AF, Alexa Fluor.

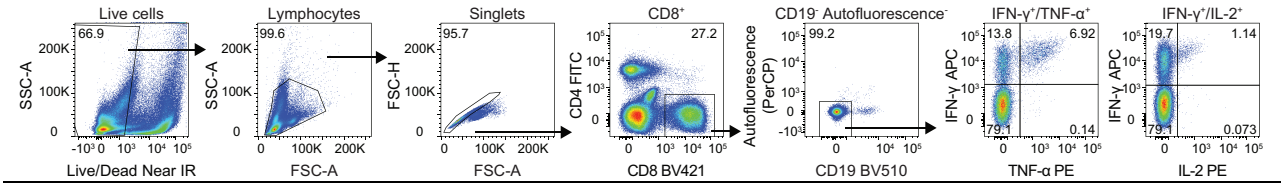

Supplementary Fig. 7. Gating strategy for functional characterization of LCMV-specific CD8$^+$ T cells in Fig. 5c, 6c, Extended Data Fig. 1c, and Extended Data Fig. 10c. Splenocytes were isolated from LCMV chronically infected mice of various treatment groups. After stimulating them with pool of 9 LCMV-specific peptides for 5 hours, cells were gated on live cells, lymphocytes, singlets, CD8$^+$ T cells, autofluorescence$^-$ cells, and cytokine producing LCMV-specific CD8$^+$ T cells were analyzed. AF, Alexa Fluor.

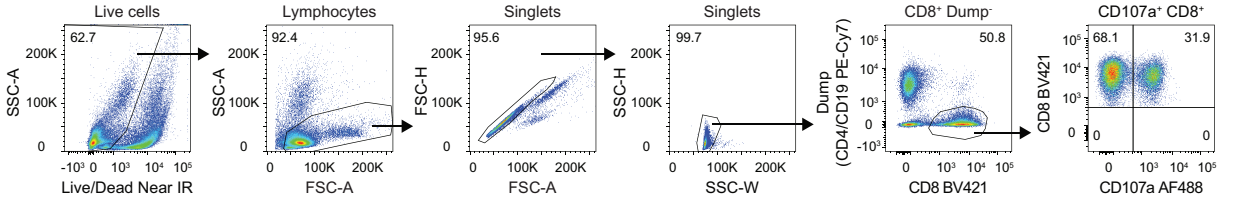

Supplementary Fig. 8. Gating strategy for functional characterization of LCMV-specific CD8$^+$ T cells in Extended Data Fig. 1d. Splenocytes were isolated from LCMV chronically infected mice of various treatment groups. After stimulating them with pool of 9 LCMV-specific peptides for 5 hours, cells were gated on live cells, lymphocytes, singlets, CD8$^+$ T cells, and degranulating LCMV-specific CD8$^+$ T cells were analyzed. AF, Alexa Fluor.

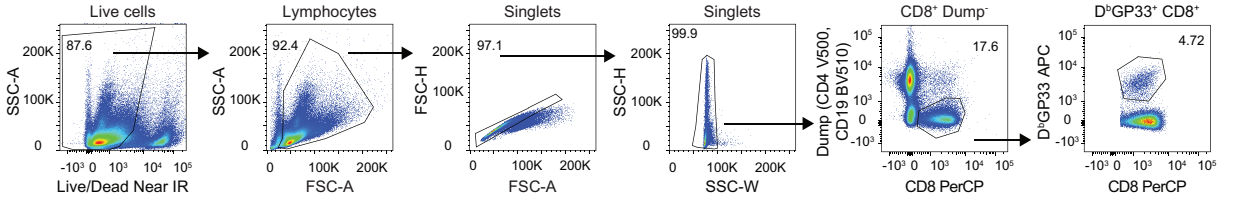

Supplementary Fig. 9. Gating strategy for LCMV-specific CD8$^+$ T cells in Extended Data Fig. 12e, f. Splenocytes isolated from LCMV chronically infected mice of various treatment groups were gated on live cells, lymphocytes, singlets, CD8$^+$ T cells, and LCMV-specific D^{b}GP33$^+$ CD8$^+$ T cells were analyzed.

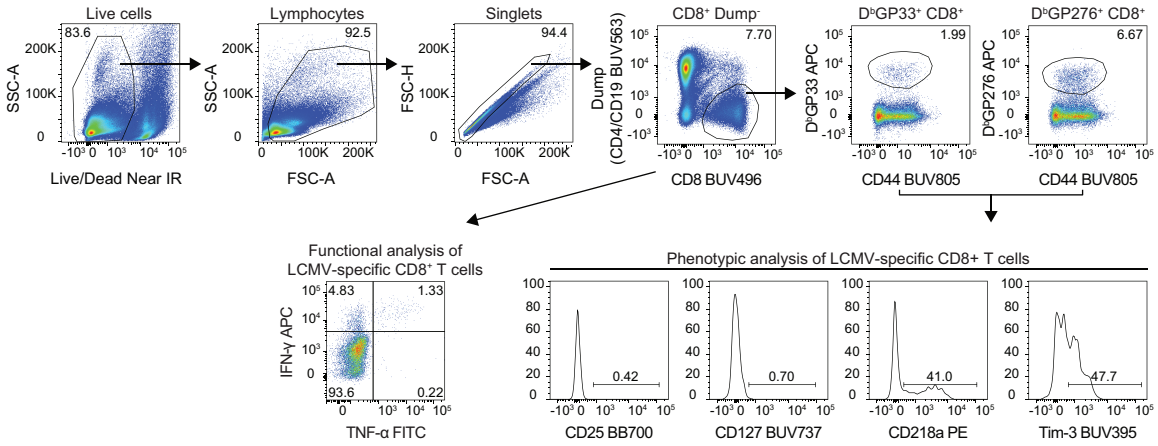

Supplementary Fig. 10. Gating strategy for LCMV-specific CD8⁺ T cells in Extended Data Fig. 13c, d. Splenocytes isolated from LCMV chronically infected mice of various treatment groups were gated on live cells, lymphocytes, singlets, CD8⁺ T cells, and LCMV-specific DᵇGP33⁺ CD8⁺ T cells were analyzed.

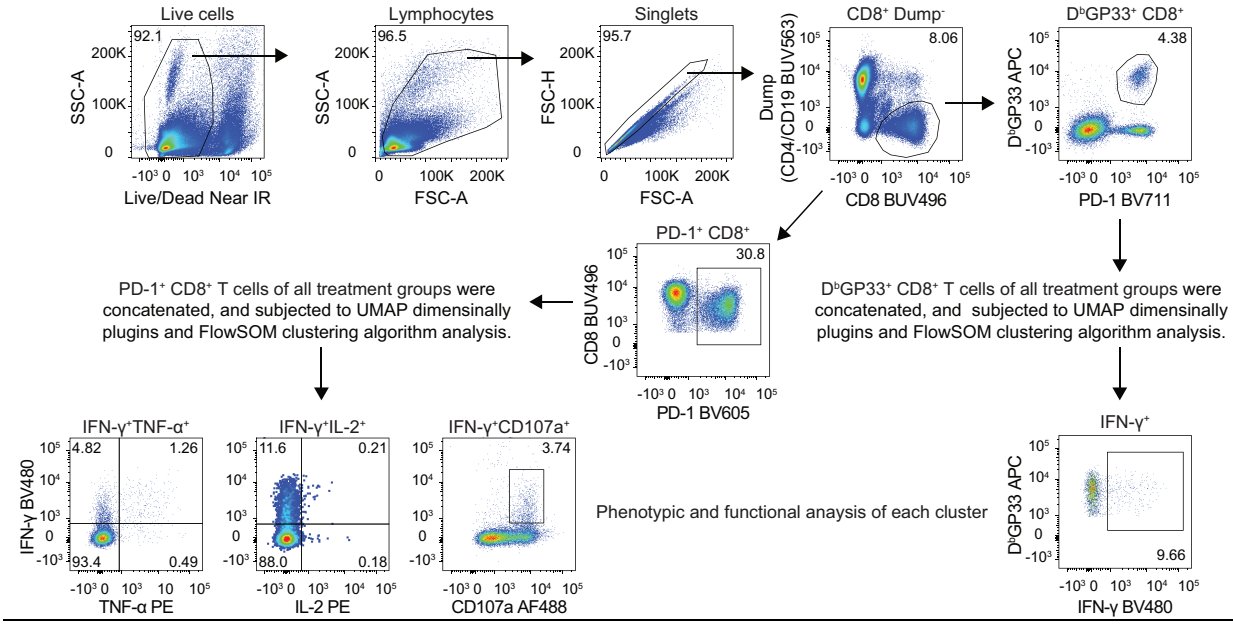

Supplementary Fig. 11. Gating strategy for phenotypic and functional characterization of LCMV-specific CD8⁺ T cells generated by PD-1, IL-2, and the combination therapy in Fig. 3a-e and Extended Data Fig. 5. Splenocytes isolated from LCMV chronically infected mice of various treatment groups were gated on live cells, lymphocytes, singlets, CD8⁺ T cells, and LCMV-specific PD-1⁺ CD8⁺ T cells or DᵇGP33⁺ CD8⁺ T cells or were analyzed. AF, Alexa Fluor.

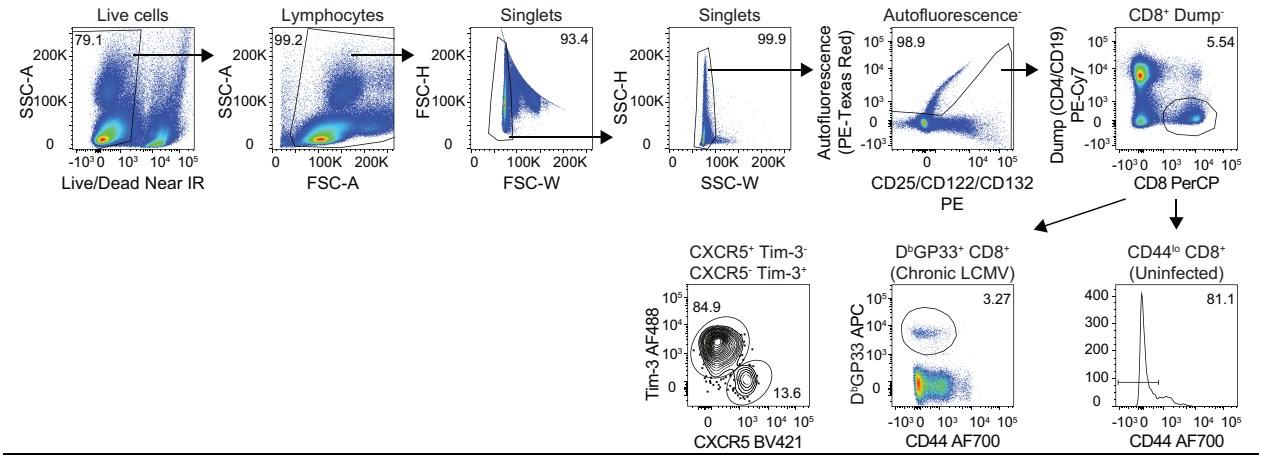

Supplementary Fig. 12. Gating strategy for analyzing IL-2 receptor expression on stem-like (CXCR5$^+$Tim-3$^-$) and exhausted (CXCR5$^-$Tim-3$^+$) CD8$^+$ T-cell subset in D^{b}GP33$^+$ CD8$^+$ T cells and naive CD8$^+$ T cells in Extended Data Fig. 9g, 9j, and 9m. Splenocytes isolated from chronically LCMV-infected mice or uninfected C57BL/6J mice were gated on live cells, lymphocytes, singlets, autofluorescence$^-$ cells, and CD8$^+$ were identified. Two subsets of D^{b}GP33$^+$ CD8$^+$ T cells in chronically LCMV-infected mice and CD44^{lo} CD8$^+$ T cells in uninfected C57BL/6J mice were analyzed for IL-2 receptor expression. AF, Alexa Fluor.

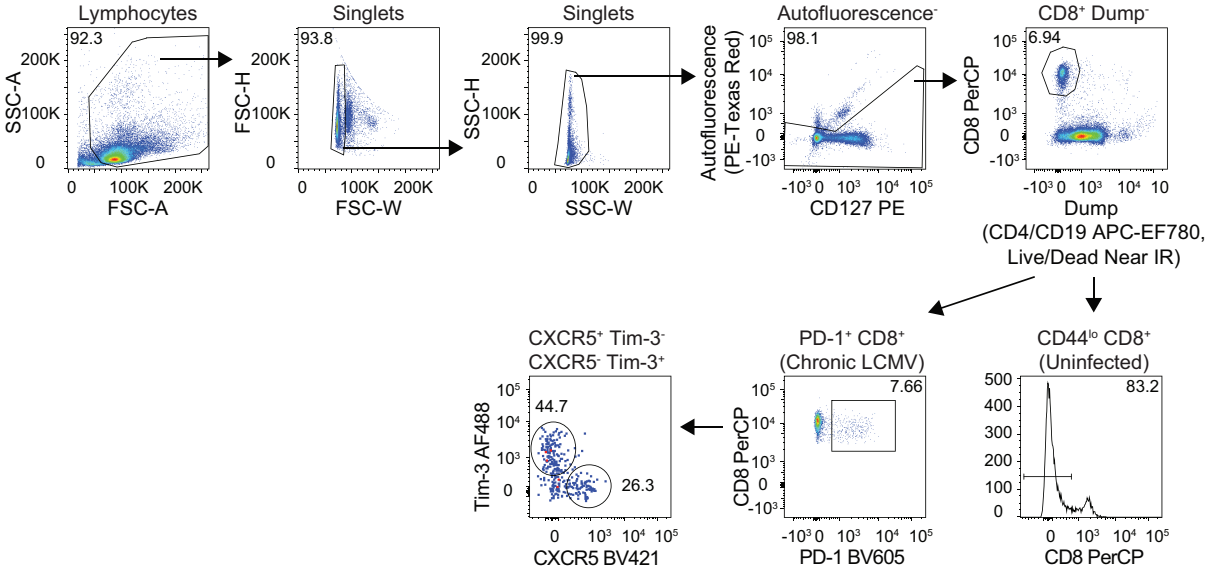

Supplementary Fig. 13. Gating strategy for analyzing CD25 expression on stem-like (CXCR5$^+$Tim-3$^-$) and exhausted (CXCR5$^-$Tim-3$^+$) CD8$^+$ T-cell subset in PD-1$^+$ CD8$^+$ T cells and naive CD8$^+$ T cells in Extended Data Fig. 9b. Splenocytes isolated from chronically LCMV-infected mice or uninfected C57BL/6J mice were gated on live cells, lymphocytes, singlets, autofluorescence$^-$ cells, and live CD8$^+$ were identified. Two subsets of D^{b}GP33$^+$ CD8$^+$ T cells in chronically LCMV-infected mice and CD44^{lo} CD8$^+$ T cells in uninfected C57BL/6J mice were analyzed for CD25 expression. AF, Alexa Fluor; EF, eFluor.

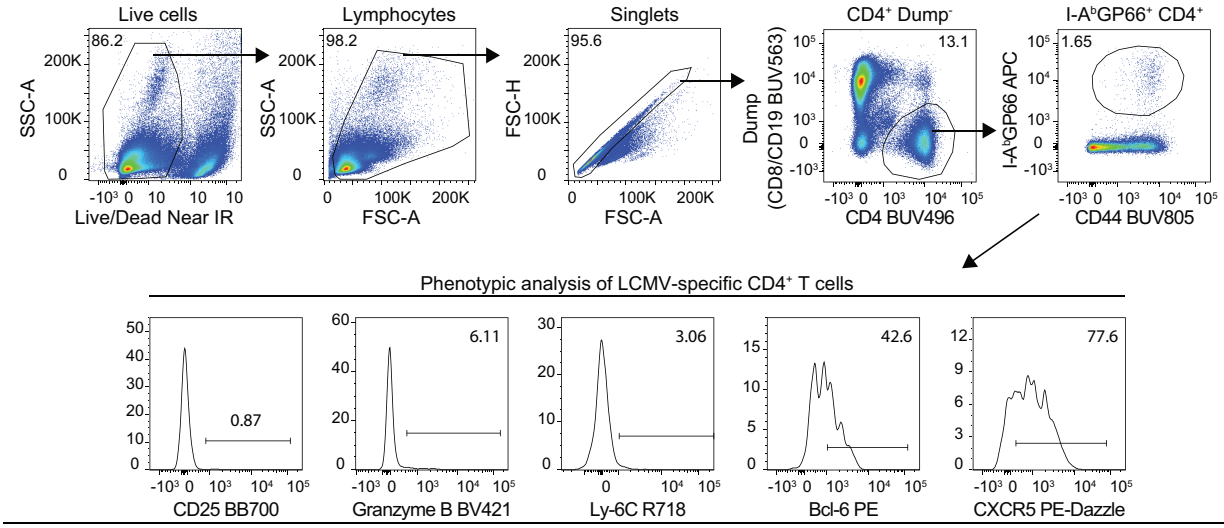

Supplementary Fig. 14. Gating strategy for LCMV-specific CD4$^+$ T cells in Extended Data Fig. 13f. Mice were infected with LCMV clone 13. At day 25 post-infection, they were left untreated, or treated with anti-PD-L1 antibody, anti-PD-L1 plus IL-2wt, or anti-PD-L1 plus IL-2v. Splenocytes were isolated at day 34 post-infection, gated on live cells, lymphocytes, singlets, CD4$^+$ T cells, and LCMV-specific I-A^{b}GP66$^+$ CD4$^+$ T cells were identified.

T cell analysis (donor CD45.2$^+$ CD8$^+$ T cells in adoptive transfer experiments)

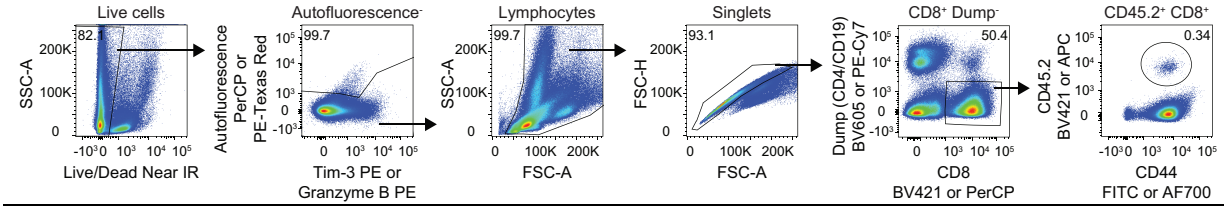

Supplementary Fig. 15. Gating strategy for donor CD45.2$^+$ CD8$^+$ T cells in Fig. 1b, c, Extended Data Fig. 2b-d, and Extended Data Fig. 9c, d. Cells isolated from various tissues in LCMV chronically infected recipient mice (CD45.1$^+$) of different treatment groups were gated on live cells, autofluorescence$^-$ cells, lymphocytes, singlets, CD8$^+$ T cells, and donor CD45.2$^+$ CD8$^+$ T cells were analyzed for their frequency and CD25 expression. AF, Alexa Fluor.

Supplementary Notes

Supplementary Data 1. Functional significance of cis-regulatory regions more open in LCMV-specific CD8$^+$ T cells after PD-1/IL-2 combination therapy compared to PD-1 monotherapy. Functional significance of cis-regulatory regions in DbGP33$^+$ CD8$^+$ T cells is defined by using ATAC-seq data and genomic regions enrichment of annotations tool (GREAT)[26] between PD-1 monotherapy and the combination therapy. Gene Ontology (GO) terms identified by open regions for the combination therapy are listed. The p-values reported by GREAT were calculated using a hypergeometric test on chromosome coordinates of the peaks for the corresponding comparisons (foreground) compared to all consensus peaks (background).

Supplementary Data 2. Functional significance of cis-regulatory regions more closed in LCMV-specific CD8$^+$ T cells after PD-1/IL-2 combination therapy compared to PD-1 monotherapy. Functional significance of cis-regulatory regions in DbGP33$^+$ CD8$^+$ T cells is defined by using ATAC-seq data and genomic regions enrichment of annotations tool (GREAT)[26] between PD-1 monotherapy and the combination therapy. Gene Ontology (GO) terms identified by closed regions for the combination therapy are listed. The p-values reported by GREAT were calculated using a hypergeometric test on chromosome coordinates of the peaks for the corresponding comparisons (foreground) compared to all consensus peaks (background).

Supplementary Data 3. Transcription factor family members regulating chromatin accessibility in LCMV-specific CD8$^+$ T cells in acute and chronic infection and after PD-1/IL-2 combination therapy. The lists of transcription factor family members determined by HOMER analysis[57] that are highly accessible to differentially accessible regions in each of the 10 clusters of Extended Data Fig. 6c. The p-values reported by HOMER[57] were calculated using a hypergeometric test for enrichment of the motif in the sequences of the peaks for the corresponding comparisons (target/foreground) compared to that motif's enrichment in the sequences of the peaks not significantly different.